A Novel DE algorithm for Solving Uncertainty-Inclusive Operational Expected Security Cost Problems with Flexible Resources in Smart grids

B. Aruna Kumari[1*], K. Vaisakh[2], N.C.Sahoo[3]

[1*] Department of Electrical Engineering, Andhra University College of Engineering (A), Visakhapatnam-530003, A.P, India.
[2] Department of Electrical Engineering, Andhra University College of Engineering (A), Visakhapatnam-530003, A.P, India.
[3] School of Electrical Sciences, Indian Institute of Technology, Bhubaneswar-752050, ODISHA, India.

* Corresponding author

Abstract

Integrating uncertainties from renewable energy resources (RER) such as wind and solar-based power generation, combined with the dwindling fossil fuel generation and rapidly changing energy demand, pose significant operational and security concerns for modern power networks. This paper presents a "Novel Differential Evolution (NDE)" algorithm for an uncertainty-inclusive, expected security cost dynamic optimal power flow (ESCDOPF) model that incorporates flexible resources (FR). The algorithm is developed based on a new crossover operator and a new local control strategy with a small population size. The main objective of this research work is to obtain a global solution for the total operating cost that meets the operational constraints during the day. The RER uncertainties are modelled through Weibull and Beta probability distribution functions (PDFs) and also FRs such as battery energy storage systems (BESS) and mesh-connected multi-terminal HVDC systems are modelled to enhance security and reliability. The effectiveness of the proposed NDE algorithm is illustrated in two different scenarios on an IEEE 30 system while considering with and without RER along with different combinations of FR. Results show that the ESCDOPF model incorporating RER and FR helps to minimise the total operation cost under normal and post-contingency conditions.

Keywords

Dynamic optimal power flow, battery energy storage systems, expected security cost, flexible resources, multi-terminal HVDC systems, N-1 security, novel differential evolution algorithm

1. Introduction

The integration of renewable energy resources (RER)-based power generation, combined with dwindling fossil fuel generation and ever-changing energy demand, poses significant operational and security challenges for modern power systems [1]. The overarching goal of modern power system operations is to securely dispatch and efficiently serve the load while integrating diverse generation technologies. Optimal power flow (OPF) is an important issue in power system dispatching and security. The OPF model faces the challenge of balancing the needs of the transmission network while minimising operating costs [2].

In [3], the authors proposed dynamic optimal power flow (DOPF), an extended method for solving OPF over a time horizon by incorporating inter-temporal constraints. The AC security-constrained OPF (SCOPF) [4]–[5] is a tool for ensuring N-1 security that is primarily used in day-to-day operations to procure ancillary services. Based on the SCOPF paradigm, there are two methods, i.e., preventive SCOPF and corrective SCOPF. Several literature reviews have been carried out to enhance security against the state of post-contingency in both preventive and corrective SCOPFs [6]–[7]. The authors of [8] have presented a formulation that minimises the total expected operating cost, as well as the post-contingency generation rescheduling and load interruption costs, minus the customer benefits. To solve the model with dc approximation, the primal-dual interior-point (PDIP) algorithm is used. This model was later extended to include AC networks with small-signal stability constraints [9]. Because of environmental concerns and recent energy shortages, the incorporation of RER (i.e., wind and solar) is becoming more popular [10]. Due to the stochastic nature of the RER, the management of uncertainty and variability in the RER is a crucial challenge. Thus,

extant literature reveals that several literature studies have been reported on the formation of economic dispatch (ED) [11]–[12], OPF [13]–[17] and SCOPF [18] with RER using different heuristic algorithms. The electricity market creates a flexible resource (FR) for operating a secure and reliable system in real-time situations due to the continuous increase in demand and rapid development of the smart grid [19]. Battery energy storage systems (BESS) and high voltage direct current (HVDC) systems are commonly used FR to enhance security and reliability.

BESS is a form of scalable resource that has recently attracted a lot of attention from researchers, system operators, and end-users [20]–[22]. Due to the rapid decline in the cost of storage technologies, especially lithium-ion batteries, the role of battery storage in a power system has gained prominence [23]. Its main purpose is to conserve the stored resources and it plays an important role in ensuring that supply and demand are balanced at all times. The BESS is mainly concerned with energy efficiency in order to reduce costs and increase revenue while maintaining flexibility. As part of the solution to the SCOPF, the authors of [24] propose that batteries operate in the post-contingency corrective control state. In [25], the authors studied the DOPF problem of active distribution networks containing RER, flexible demand and energy storage systems (ESS) in an active network management context. In [26], a stochastic MP-SCOPF with flexible loads and ESS to provide flexibility for regulating congestion and voltages has been proposed.

Due to the grid's controllability and reliability by enabling transmission over longer distances with less power loss, the line commutated converters (LCC)-HVDC systems seem to be the most secure and cost-effective choice [27]–[32]. The authors of [33] describe a decoupled way of computing multi-period (MP) SCOPF that covers both N-1 security criteria and quasi-stationary dynamics in smart grids with ESS via interconnected area coordination.

As previously stated, only a few authors aiming to extend AC SCOPF have analysed emerging sources of flexibility in conjunction with RER uncertainties. Despite these encouraging developments, this paper proposes a new mathematical approach for extending the MP-SCOPF model by considering security as an economic cost rather than a constraint, colloquially referred to as "expected security cost DOPF" (ESC-DOPF), to minimise expected system operating costs under pre/normal and post-contingencies. To the best of the authors' knowledge, the researchers have not addressed the formulation of the problem in the form of an MP-ESCOPF or ESC-DOPF with the integration of RER and FR. The wind and solar stochastics' are modelled through Weibull and Beta probability distribution functions [12]–[13]. To improve the system reliability, BESS is also applied to the proposed model. Furthermore, the authors developed a unified Newton-Raphson (NR) based meshed multi-terminal line commutated converter (LCC)-HVDC system [27], [29]–[30], [32] that can be applied to the ESCDOPF model. Evolutionary algorithms are capable of effectively solving the proposed model. In recent decades, Storn and Price (1995) differential evolution (DE) algorithm has established itself as a powerful population-based stochastic search algorithm for finding a globalised solution with good global search capability and few or no cost function constraints [34]–[36]. However, because the standard DE has inherent difficulties in solving complex multi-modal problems with a high degree of dimensionality, it is encouraged to develop an effective novel DE variant. Numerous experts have proposed various control strategies for optimising the DE algorithm [37]–[40]. While all of these methods can help the standard DE perform better, they are insufficient for certain functions. To address this issue, the proposed model in this paper employs a "New Differential Evolution (NDE)" algorithm [41] to minimise the expected total operating cost. This introduces a new crossover operator and a new local adaptation approach. The proposed algorithm's robustness is verified on ESCDOPF with RER and FR during pre-and post-contingency states. Also, the economic benefits of incorporating RER and FR into the ESCDOPF model are assessed.

The rest of the paper is arranged as: Section 2 presents the formulations of the ESCDOPF model with RER and FR. Section 3 focuses on the solution methodology. Section 4 represents the simulation results with discussions, respectively. Finally, the concluding remarks are given in Section 5.

2 Formulation of ESCDOPF model with RER and FR

The detailed mathematical modelling of the proposed ESCDOPF with RER and FR is discussed in this section.

2.1 Models of renewable energy resources

In this model, the Weibull and Beta probability distribution functions (PDFs) are used to represent the wind speed (v) and solar irradiance (G_s) because it closely reflects their practical distribution, which can be found in [12]. The wind speed profile calculated by Weibull PDF ($f_W(v)$) with respect to the wind velocity function (v) m/s is as follows:

$$f_W(v) = \left(\frac{s_k}{s_c}\right)\left(\frac{v}{s_c}\right)^{(s_k-1)} (\exp)^{-(v\cdot s_c)^{s_k}} \quad ,0 < v < \infty \tag{1}$$

where s_k and s_c are the shape and scale parameters.

The output power for a given wind speed (v) by using a piece-wise linear function and is given in (2).

$$p_w(v)=\begin{cases}0, & for\ v<v_{in}\ and\ v>v_{out}\\ p_{wr}\left(\dfrac{v-v_{in}}{v_{wr}-v_{in}}\right) & for\ v_{in}\le v\le v_{wr}\\ p_{wr} & for\ v_{wr}<v\le v_{out}\end{cases} \quad (2)$$

Here, wind speeds are taken as cut-in speed (v_{in}), cut-out speed (v_{out}) and rated speed (v_{wr}) respectively; (p_{wr}) is the rated output power.

The output of a PV generator can be found in [12]. The probability of solar irradiance (G_s) can be calculated by Beta PDF ($f_{G_s}(G_s)$) as follows [12]:

$$f_{G_s}(G_s)=\begin{cases}\dfrac{\Gamma(a_s+b_s)}{\Gamma(a_s)\Gamma(b_s)}\left(\dfrac{G_s}{G_{max,s}}\right)^{a_s-1}\left(1-\dfrac{G_s}{G_{max,s}}\right)^{b_s-1}; & for\ 0\le\left(\dfrac{G_s}{G_{max,s}}\right)\le 1,\quad a_s>0, b_s>0,\\ 0\ ;\ \ Otherwise\end{cases} \quad (3)$$

where a_s and b_s are the beta parameters with mean μ_s and standard deviation σ_s is as follows

$$a_s=\mu_s^2\left(\frac{1-\mu_s}{\sigma_s^2}-\frac{1}{\mu_s}\right);\quad b_s=a_s\left(\frac{1}{\mu_s}-1\right) \quad (4)$$

Since, the Beta distribution variable lies in the range of (0, 1). Hence, a nominal value of solar irradiance is (G_s/ $G_{max,s}$) considered. where $G_{max,\,s}$ is the maximum solar irradiance. Further, the solar irradiance to energy conversion for solar is given by:

$$f_{G_s}(P_s)=\begin{cases}\dfrac{1}{P_{max,s}}\dfrac{\Gamma(a_s+b_s)}{\Gamma(a_s)\Gamma(b_s)}\left(\dfrac{P_s}{P_{max,s}}\right)^{a_s-1}\left(1-\dfrac{P_s}{P_{max,s}}\right)^{b_s-1}; & \text{for}\ \ 0\le\left(\dfrac{P_s}{P_{max,s}}\right)\le 1,\quad a_s>0, b_s>0,\\ 0;\ \ otherwise\end{cases} \quad (5)$$

where $P_{max,s}$ is the maximum generated solar power; P_s is the solar power.

2.2 Models of flexible resources

From power generation to better transmission and distribution networks, this flexibility must be applied across the energy system. Flexibility resource services may be categorised using the idea of energy security and management [19]. The following are some of the most in-depth discussions:

2.2.1 Battery Energy Storage System (BESS) model

For the sake of simplicity, BESS is lossless and operates at a unity power factor. In this model, three modes of operation have been considered [20–21]. In the first mode, excess generation charges the battery, which acts as a load. Assuming there is no battery, generation equals demand, and the battery remains saturated at its maximum/minimum state-of-charge (SOC) levels. To meet demand in the third mode, the battery discharges and acts as a generator. The SOC is determined by multiple time steps of charge and discharge values.

The following are the battery charging and discharging equations [21] as:

$$SOC_{b,t}^{k} = \begin{cases} SOC_{b,t}^{ini,k}, & t = 1 \\ SOC_{b,t-1}^{k} + \left(U_{ch_b,t-1} * P_{ch_b,t-1}^{k} * \eta_{ch_b}\right) - \left(U_{dch_b,t-1} * \frac{P_{dch_b,t-1}^{k}}{\eta_{dch_b}}\right)\Delta t, & b \in N_{batt}, t > 1 \end{cases} \quad (6)$$

$$\sum_{t} P_{dch_b,t}^{k} \Big/ \eta_{dch_b} - \sum_{t} P_{ch_b,t}^{k} \cdot \eta_{ch_b} = 0 \quad \forall k \in (0,1,....,K) \quad (7)$$

$$U_{ch_b,t} + U_{dch_b,t} \leq 1, \ \forall b, t \quad (8)$$

The energy stored inside the battery at each time interval t is given in (6). Whereas Eq. (7) is used to distinct each day from the others. Eq. (8) defines the ability to load or unload at the same time. Here, k=0 and k>0 indicate the pre/normal contingency(C) state and post-contingency (C) states; K is the total number of contingencies; $P_{ch_b,t}^{k}$ and $P_{dch_b,t}^{k}$ are the b^{th} battery-charging (ch) and discharging (dch) powers of the k^{th} contingency state at time t respectively. $U_{ch_b,t}$ / $U_{dch_b,t}$ are the battery charging /discharging status. η_{ch_b} and η_{dch_b} are the charging and discharging efficiencies.

2.2.2 Unified HVDC NR model

In this study, a unified HVDC/AC-DC approach based on the Newton-Raphson (NR) algorithm with mesh connected multi-terminal (MT) line commutated converter (LCC) configurations is developed for evaluating power flow in an ESCDOPF model. In this model, the AC and DC power flow solutions can be solved simultaneously by the NR algorithm with a modified jacobian matrix [29]. The power flow equations of AC-DC systems are briefly described in the following subsection for rapid reference. The complete unified power flow model can be simplified using first order Taylor expansion is given as:

$$\Delta F_{ac-dc}^{k} = -J_{ac-dc}^{k} \ \Delta X_{ac-dc}^{k} \quad (9)$$

Where ΔF_{ac-dc}^{k} is the residual of AC-DC system power flow equations; J_{ac-dc}^{k} are the jacobian matrix of ΔF_{ac-dc}^{k} ΔX_{ac-dc}^{k} are the corrections for the AC-DC solutions, respectively.

2.3 Objective function

The classic ESCOPF formulation, which was originally proposed in [8], is adopted in this paper. This classic approach, however, implies that control operations do not change during an emergency. Many resources, such as RER and FR, have recently been implemented in the system since their inclusion can operate as a preventive control measure during contingency periods and improve the system's performance in a safe, reliable, and economical manner. The main objective is to minimise the expected system operating cost by satisfying the model constraints in transmission network operation under both pre-and post-contingency states.

This ESCDOPF problem can be abstractly and generically formulated as follows:

$$\min_{C^k} \left\{ ESC = \left(\sum_{k=0}^{K} \sum_{t=1}^{T} \pi^k \ C^k(t) \right) \right\} \ \forall k = \{0,1,.....K\} \quad (10)$$

where $C^k(t)$ is the expected operating cost, which includes pre/normal and post-contingency operating costs over a time interval T; The term "expected" is used in a probabilistic manner, and it applies to all contingencies; The probability of a contingency k is denoted as π^k [8].

The ESCDOPF problem with different cost models can be explicitly expressed as follows:

$$C^k(t) = \underbrace{C_{G_i}(P^k_{G_i,t})}_{GC} + \underbrace{C_w(P^k_{w,t})}_{WC} + \underbrace{C_s(P^k_{s,t})}_{SC} + \underbrace{H_b(SOC^k_{b,t})}_{BC} - \underbrace{B_{L_i}(P^k_{L_i,t})}_{CC} \quad (11)$$

2.4. Cost models

2.4.1 Generator Cost (GC) model

In this model, the valve point effects are considered. The valve loading effect is modelled as an absolute value with a sinusoidal function, which is then applied to the quadratic cost function [3] as,

$$GC = C_{G_i}(P^k_{G_i,t}) = \sum_{t=1}^{T}\sum_{i=1}^{N_G}\left(a_{G_i}\left(P^k_{G_i,t}\right)^2 + b_{G_i}P^k_{G_i,t} + c_{G_i} + \left|d_{G_i}\cdot sin(e_{G_i}(P^{\min}_{G_i} - P^k_{G_i}))\right|\right) \quad (12)$$

Where a_{G_i}, b_{G_i}, c_{G_i}, d_{G_i} and e_{Gi} are the coefficients of generator (G) cost functions with valve loading effect. $P^k_{G_i,t}$ is the output power of the i[th] generating unit of k[th] contingency at time 't' in MW. $P^{\min}_{G_i}$ is the generating unit's minimum real power in MW; N_G is the number of generating units.

2.4.2 Wind Cost (WC) Model

In this model, to incorporate the uncertain effect, the operating costs of wind generators include direct wind cost, underestimation/penalty cost and overestimation/ reserve cost. Wind power has a direct cost associated to it. When the cost of underestimation is taken in to account, the available wind power is more than the estimated wind power. But at an overestimation cost, the available wind power is less than the estimated wind power. Therefore, penalties have been introduced for the unused power. The wind operating cost ($C_w(P^k_{w,t})$) of w[th] wind generator to generate wind power ($P^k_{w,t}$ MW) at time interval 't' with 'N_W' number of wind-generating units can be described [12] as,

$$WC = C_w(P^k_{w,t}) = \sum_{t=1}^{T}\sum_{w=1}^{N_W}\left[C^k_{w,t} + C^k_{pw,t} + C^k_{rw,t}\right] \quad (13)$$

The wind direct cost (14), penalty cost (15) and reserve cost (16) can be expressed as:

$$C^k_{w,t} = K_w \times P^k_{w,t} \quad (14)$$

$$C^k_{pw,t} = K_{pw}\int_{P^k_{w,t}}^{P_{wr}}\left(p^k_{w,t} - P^k_{w,t}\right)f_w\left(p^k_{w,t}\right)dp^k_{w,t} \quad (15)$$

$$C^k_{rw,t} = K_{rw}\int_{0}^{P^k_{w,t}}\left(P^k_{w,t} - p^k_{w,t}\right)f_w\left(p^k_{w,t}\right)dp^k_{w,t} \quad (16)$$

Where $f_w\left(p^k_{w,t}\right)$ is the PDF of wind power at time t; K_w, K_{pw} and K_{rw} are the direct wind, penalty, reserve cost coefficients for w[th] wind power plant;

2.4.3 Solar Cost (SC) Model

The solar operating cost ($C_s(P^k_{s,t})$) of s[th] solar generator to generate solar power ($P^k_{s,t}$) at a time interval 't' with 'N_S' number of solar-generating units can be described [12] as,

$$SC = C_s(P^k_{s,t}) = \sum_{t=1}^{T}\sum_{s=1}^{N_S}\left[C^k_{s,t} + C^k_{ps,t} + C^k_{rs,t}\right] \quad (17)$$

The solar direct cost (18), penalty cost (19) and reserve cost (20) can be expressed as follows:

$$C_{s,t}^{k} = K_s \times P_{s,t}^{k} \tag{18}$$

$$C_{ps,t}^{k} = K_{ps} \int_{P_{s,t}^{k}}^{P_{sr}} \left(p_{s,t}^{k} - P_{s,t}^{k} \right) f_s \left(p_{s,t}^{k} \right) dp_{s,t}^{k} \tag{19}$$

$$C_{rs,t}^{k} = K_{rs} \int_{0}^{P_{s,t}^{k}} \left(P_{s,t}^{k} - p_{s,t}^{k} \right) f_s \left(p_{s,t}^{k} \right) dp_{s,t}^{k} \tag{20}$$

Where $f_s\left(p_{s,t}^{k}\right)$ is the PDF of solar power at time t. K_s , K_{ps} and K_{rs} are the direct solar, penalty, reserve cost coefficients for s^{th} solar power plant;

2.4.4 Battery-Storage Cost (BC) Model

In this model, we assume that battery cost is independent of power draw (P_b) but dependent on energy storage level ($SOC_{b,t}^{k}$) [20] with the total number of batteries N_{batt} as given in (21).

$$BC = H_b(SOC_{b,t}^{k}) = \sum_{t=1}^{T} \sum_{b=1}^{N_{batt}} h_b \left(SOC_{b\max} - SOC_{b,t}^{k} \right) \tag{21}$$

Where $SOC_{b\max}$ is the maximum storage capacity of a battery and h_b imposes a penalty proportional to the stored energy level's deviation from the unit capacity on the battery's cost function.

2.4.5 Consumer-Benefit Cost (CC) Model

This model represents the benefit cost, which is obtained from the benefit-cost curve as a function of real power consumption as given in (22). Here, the load is treated as price-based demand, and social welfare (SW) is defined as consumer benefit costs minus producer costs. Moreover, these consumer benefit costs are treated as negative costs into an objective function. Thus, there would be an increase in social welfare or a reduction in the expected total cost [8].

$$CC = B_{L_i}(P_{L_i,t}^{k}) = \sum_{t=1}^{T} \sum_{i=1}^{N_L} a_{L_i} \left(P_{L_i,t}^{k} \right)^2 + b_{L_i} P_{L_i,t}^{k} + c_{L_i} \tag{22}$$

Where a_{L_i}, b_{L_i} and c_{L_i} are the coefficients of the benefit-cost functions; N_L is the total number of load buses; $P_{L_i,t}^{k}$ is the load demand power.

2.5 Constraints

2.5.1 AC Power flow constraints

The real and reactive power balance equations are given as follows:

$$\left.\begin{aligned} P_{i,t}^{k} &= P_{G_i,t}^{k} + P_{w,t}^{k} + P_{s,t}^{k} - P_{ch_b,t}^{k} + P_{dch_b,t}^{k} - P_{L_i,t}^{k} \\ Q_{i,t}^{k} &= Q_{G_i,t}^{k} - Q_{L_i,t}^{k} \end{aligned}\right\} \tag{23}$$

$$\forall\, i, w, s, b, k, t \in T,$$

The calculated real ($P_{i,t}^{k}$) and reactive ($Q_{i,t}^{k}$) powers at time (t) are given as:

$$\left.\begin{aligned} \mathrm{P}_{i,t}^{k} &= \mathrm{V}_{i,t}^{k} \sum_{j=1}^{N_{bus}} \mathrm{V}_{j,t}^{k} \left[G_{ij} \cos\left(\theta_{ij,t}^{k}\right) + B_{ij} \sin\left(\theta_{ij,t}^{k}\right) \right] \\ Q_{i,t}^{k} &= \mathrm{V}_{i,t}^{k} \sum_{j=1}^{N_{bus}} \mathrm{V}_{j,t}^{k} \left[G_{ij} \sin\left(\theta_{ij,t}^{k}\right) - B_{ij} \cos\left(\theta_{ij,t}^{k}\right) \right] \end{aligned}\right\} \mathrm{i} \in \mathrm{N_{bus}} \tag{24}$$

Where $Q_{G_i,t}^{k}$ and $Q_{L_i,t}^{k}$ are the i^{th} reactive power output and reactive load demand in MVAR; voltage magnitude and difference in phase angle are $V_{i,t}^{k}$ and $\theta_{ij,t}^{k} = \theta_{i,t}^{k} - \theta_{j,t}^{k}$; G_{ij} and B_{ij} are the conductance and susceptance between buses i and j, respectively; $\mathrm{N_{bus}}$ is the total number of buses.

Thermal generator boundary limits: The active power and reactive power generation limits, and also generator voltage limits are given as [3]:

$$\left.\begin{aligned} P_{G_i}^{\min} &\le P_{G_i,t}^{k} \le P_{G_i}^{\max} \\ Q_{G_i}^{\min} &\le Q_{G_i,t}^{k} \le Q_{G_i}^{\max} \\ V_{G_i}^{\min} &\le V_{G_i,t}^{k} \le V_{G_i}^{\max} \end{aligned}\right\}, \forall i \in \{1,2,3,...N_G\} \tag{25}$$

Transformer taps setting constraints:

$$\mathrm{k}_{\mathrm{A}\min}^{\mathrm{k}} \le \mathrm{k}_{\mathrm{A,t}}^{\mathrm{k}} \le \mathrm{k}_{\mathrm{A}\max}^{\mathrm{k}}, \forall \mathrm{A} \in \{1,\ldots\ldots \mathrm{N_{rt}}\} \tag{26}$$

Where $\mathrm{N_{rt}}$ is the total number of regulating transformers

Reactive power injections constraints:

$$\mathrm{Q}_{\mathrm{c}_{\min}}^{\mathrm{k}} \le \mathrm{Q}_{\mathrm{c,t}}^{\mathrm{k}} \le \mathrm{Q}_{\mathrm{c}_{\max}}^{\mathrm{k}}, \forall \mathrm{c} \in \{1,\ldots\ldots \mathrm{N_{cap}}\} \tag{27}$$

where $\mathrm{N_{cap}}$ is the total number of shunt capacitors.

Security Constraints: Load bus voltages and transmission line loadings are examples of these constraints, which can be stated as,

$$\left.\begin{aligned} \mathrm{V}_{\mathrm{L}_{\min}}^{\mathrm{k}} &\le \mathrm{V}_{\mathrm{L,t}}^{\mathrm{k}} \le \mathrm{V}_{\mathrm{L}_{\max}}^{\mathrm{k}}, \forall \mathrm{L} \in \{1,2,3,\ldots\ldots \mathrm{N_L}\} \\ \mathrm{S}_{\mathrm{l,t}}^{\mathrm{k}} &\le \mathrm{S}_{\mathrm{l}_{\max}}, \forall \mathrm{l} \in \{1,2,3,\ldots\ldots \mathrm{N_{trl}}\} \end{aligned}\right\} \tag{28}$$

where $\mathrm{N_{trl}}$ denotes the total number of transmission lines.

Ramp-up and down limits of generating limits: The ramp up and down limits are given as:

$$\left.\begin{aligned} P_{G_i,t+1}^{\max} &= min\left(P_{G_i}^{\max}, P_{G_i,t}^{k} + RU_i\right) \\ P_{G_i,t+1}^{\min} &= max\left(P_{G_i}^{\min}, P_{G_i,t}^{k} - RD_i\right) \end{aligned}\right\} \tag{29}$$

where $\mathrm{RU_i}$ and $\mathrm{RD_i}$ are the up and down ramp rate limits of i^{th} generating unit in MW per hour respectively.

Prohibited zones operating limits [3]: In prohibited areas, generating unit operation is usually avoided are as follows:

$$P_{G_i,t}^{k} \in \begin{cases} P_{Gi}^{\min} \le P_{G_i,t}^{k} \le P_{i,1}^{L} & \text{or} \\ P_{i,n_z-1}^{U} \le P_{G_i,t}^{k} \le P_{i,n_z}^{L} & \text{or} \\ P_{i,n_{pz}}^{U} \le P_{G_i,t}^{k} \le P_{G_i}^{\max} & \mathrm{n}_z = 2,3,....,\mathrm{n}_{pz} \end{cases} \tag{30}$$

where $\mathrm{n_z}$ is the index of prohibited zones in the $\mathrm{i^{th}}$ generating unit, the number of prohibited operating zones in the $\mathrm{i^{th}}$

generating unit is expressed by n_{pz} ; $P_{i,n}^{L}$ and $P_{i,n}^{U}$ are the upper and lower boundaries of i^{th} unit, n_z^{th} prohibited operating zone in MW.

Voltage Stability Index [40]:

$$L_{l,t}^{k} \le L_{l,\max}, \forall l \in \{1,\ldots\ldots N_{trl}\} \tag{31}$$

BESS constraints: The battery storage limits, charging, and discharging power limits are given as:

$$\left.\begin{aligned} &SOC_b^{\min} \le SOC_{b,t}^{k} \le SOC_b^{\max} \\ &P_{ch_b}^{\min} \le P_{ch_b,t}^{k} \le P_{ch_b}^{\max} \\ &P_{dch_b}^{\min} \le P_{dch_b,t}^{k} \le P_{dch_b}^{\max} \end{aligned}\right\}, b \in N_{batt}, t \in T \tag{32}$$

Wind power constraints:

$$0 \le \mathrm{P}_{\mathrm{w,t}}^{\mathrm{k}} \le \mathrm{P}_{\mathrm{w}_{\max}}^{\mathrm{k}}, \forall\ \mathrm{w} \in \{1,\ldots\ldots \mathrm{N_w}\} \tag{33}$$

Solar power constraints:

$$0 \le \mathrm{P}_{\mathrm{s,t}}^{\mathrm{k}} \le \mathrm{P}_{\mathrm{s}_{\max}}^{\mathrm{k}}, \forall \mathrm{s} \in \{1,\ldots\ldots \mathrm{N_s}\} \tag{34}$$

2.5.2 AC-DC Power flow constraints

In existing HVDC-link into the AC system, the converter terminal AC buses mismatch equations are modified as [32]:

$$\left.\begin{aligned} P_{i,t}^{k} &= P_{G_i,t} + P_{w,t}^{k} + P_{s,t}^{k} - P_{ch_b,t}^{k} + P_{dch_b,t}^{k} - P_{L_i,t}^{k} - V_{D_y,t}^{k} I_{D_y,t}^{k} sign(y) \\ Q_{i,t}^{k} &= Q_{G_i,t} - Q_{L,t} - V_{D_y,t}^{k} I_{D_y,t}^{k} \tan\left(\varphi_{D_y,t}^{k}\right) \end{aligned}\right\} \tag{35}$$

On the DC side, where Nc is the number of converter buses, the DC voltage, current and power factor angle are $V_{D_y,t}^{k}$, $I_{D_y,t}^{k}$ and $\varphi_{D_y,t}^{k}$ respectively. The converter would act either as a rectifier (R) or an inverter (I) depending on whether sign convention ($sign(y)$) is +1 or -1.

2.5.3 DC System constraints

Generally, DC system model equations contain converter voltages, DC network equations and control equations such as specified DC voltage, firing angle can be summarised as follows [32]:

$$\left.\begin{aligned} &V_{D_y,t}^{k} - k_{D_y,t}^{k}\ V_{i,t}^{k} \cos\phi_{D_y,t}^{k} + X_{c_y} I_{D_y,t}^{k} = 0 \\ &V_{D_y,t}^{k} - k_{\gamma} k_{D_y,t}^{k} V_{i,t}^{k} \cos\varphi_{D_y,t}^{k} = 0 \\ &sign(y) I_{D_y,t}^{k} - \sum_{j=1}^{n_c} g_{D_y j} V_{D_y,t}^{k} = 0 \\ &V_{D_y,t}^{k} - V_{D_y}^{min} = 0 \\ &\cos\phi_{D_y,t}^{k} - \cos\phi_{D_y}^{min} = 0 \end{aligned}\right\} \forall y \in N_c \tag{36}$$

Where, $k_{D_y,t}^{k}$ is the converter transformer ratio; $\phi_{D_y,t}^{k}$ is the rectifier's angle with α_y firing angle; $\phi_{D_y,t}^{k}$ is the inverter's angle with γ_y extinction angle; X_{c_y} is the commutation reactance; k_{γ} is constant and is equal to 0.995 [32]; $g_{D_{yj},t}$ is the elements of DC nodes conductance matrix, respectively.

DC network constraints: The maximum and minimum limits of DC network variables are as follows:

$$\left.\begin{aligned} V_{D_y}^{min} \le V_{D_y,t}^{k} \le V_{D_y}^{max} \\ k_{D_y}^{min} \le k_{D_y,t}^{k} \le k_{D_y}^{max} \\ \phi_{D_y}^{min} \le \phi_{D_y,t}^{k} \le \phi_{D_y}^{max} \end{aligned}\right\}, \forall y \in \{1,2,3.....N_c\} \quad (37)$$

3 Proposed solution methodology

3.1 Standard Differential Evolution

The differential evolution (DE) algorithm is now commonly recognized as the most modern evolutionary algorithm for tackling a wide range of optimization problems in a set of real applications, including large-scale nonlinear, non-convex, and non-differentiable problems [34]. To promote fitness, mutation, crossover, and selection are the three main evolutionary operators employed in DE. The first two operators (mutation and crossover) are used to generate the test vectors, and the third operator (selection) selects which of the target vector and its test vector is better for the next generation based on their fitness values.

The major stages of DE are as follows:

Initialization: *Initialize all the j^{th} individuals of the i^{th} population member (u_{ij}) randomly within the limits of the given constraints in the search-space as follows*

$$u_{i,j}^{\tau_0} = u_j^{min} + rand * (u_j^{max} - u_j^{min}) , \forall j = 1,2..,M, \ \& \ i = 1,2,..,N_{pop} \quad (38)$$

Mutation: This operator is then applied in the following step based on the scaled difference between two selected individuals in the standard DE in a continuous search space. The most common mutation scheme employed in DE is expressed by the following equation:

$$mu_{ij}^{\tau+1} = u_{r_{1a}j}^{\tau} + F_s \times (u_{r_{2a}j}^{\tau} - u_{r_{3a}j}^{\tau}) \quad (39)$$

where F_s is referred to as the scaling factor in the [0, 1] range that governs the amplification of the differential variation $(u_{r_{2a}j}^{\tau} - u_{r_{3a}j}^{\tau})$, $r_{1a}, r_{2a}, r_{3a} \in [1, N_{pop}]$ are integers which are chosen randomly.

Crossover: A crossover operation is introduced after the mutation phase to increase the population's diversity. The target vector is shuffled to generate the trial vector $(co_{ij}^{\tau+1})$ with the mutant vector $(mu_{ij}^{\tau+1})$. In crossover operations, the following scheme is used:

$$co_{ij}^{\tau+1} = \begin{cases} mu_{ij}^{\tau+1}; & (rand(j) \le CR) or (j = J) \\ u_{ij}^{\tau}; & \text{Otherwise} \end{cases} \quad (40)$$

where CR is the crossover rate, the range is (0,1). J is an integer chosen at random from the range [1, M] and $rand(j)$ is a uniformly distributed stochastic number in the range of (0,1);

Selection: In DE, the selection operator evaluates whether a trail vector $\left(co_{ij}^{\tau+1}\right)$ or target vector $\left(u_i^{\tau}\right)$ will survive and advances to the next iteration depending on its objective values. As a selection operator, the following equation is defined:

$$u_i^{\tau+1} = \begin{cases} co_i^{\tau+1}; & \text{if } f\left(co_i^{\tau+1}\right) \le f\left(u_i^{\tau}\right) \\ u_i^{\tau}; & \text{Otherwise} \end{cases} \tag{41}$$

Where $f(.)$ is the key objective function to be minimised. As shown in (41), the trail vector replaces the target vector if its fitness value (Total expected operation cost) is better or equal, otherwise the next generation retains the target vector. As a result, the population is modified using these three evolutionary operators.

3.2 Proposed Novel DE algorithm

Many intelligent algorithms that are readily entrapped in a local search are highly expensive to process for large dimensionality optimization problems. There are a number of issues with the DE and its variants [37]-[39]. Increasing population diversity by combining strategies like large-scale population, multi-population strategy, and hybridization is the most common solution to these problems. Using a large-scale population and a multi-population approach, on the other hand, would significantly increase the computed amount while reducing the algorithm's convergence speed. When DE is combined with other methods, the end result is usually a very complicated algorithm.

To resolve these issues, we suggest a new small population-sized DE that combines the mutation operator, a new crossover operator, and a proposed local adaptation strategy to decrease computing costs. In addition, the CR is dynamically updated using an evolution method to balance exploration and extraction power [41]. **Figure 1** depicts the flow chart of the proposed novel DE (NDE) algorithm in detail. However, there are three important differences between the NDE and the standard DE.

(1) Prior to mutation and crossover operation, each trail vector $\left(co_i^{\tau}\right)$ is allocated to a target vector $\left(u_i^{\tau}\right)$.
(2) To improve the capability of global search, a new local control approach is introduced into the crossover operator.
(3) The parameter CR is supervised for both mutation and crossover. These differences are explored as below.

The dynamic crossover rate: In contrast to standard DE, where CR is fixed from start to end, the proposed NDE algorithm employs a dynamic CR function. CR achieves a high probability value for mutations, crossover, and local adaptation in the early stages of evolution. In the following step, CR has a low value for changing the decision parameters to obtain high - precision solutions.

The expression of CR is given as follows:

$$CR(\tau) = CR_{max} \cdot \left(\frac{CR_{min}}{CR_{max}}\right)^{\frac{\tau}{\tau_{max}}} \tag{42}$$

The local adaptation approach: The local adaptation (LA) approach is proposed to prevent local search in the early stages of evolution while still using high-precision solutions later on. This approach is based on step-disturbance and random-perturbation. Using the local adaptation rate (LAR), a trial solution can be altered in the vicinity of the current location with the help of the step-disturbance. Also, random-perturbation is used to explore new unknown regions in the feasible space with a probability of 0.1 LAR, mainly to prevent trapping in local search.

$$LAR(\tau) = LAR_{min} \cdot \left(\frac{LAR_{max}}{LAR_{min}}\right)^{\frac{\tau}{\tau_{max}}} \tag{43}$$

The adaptation step (AS) differs dynamically with the τ – iteration as shown in (44). The AS with a high value aims at exploring new areas in the initial process of evolution. As the value of τ increases, AS decreases steadily from AS_{max} to AS_{mid}.

$$AS(\tau)=\begin{cases} AS_{max}, & \tau \le \dfrac{\tau_{max}}{2} \\ AS_{mid}\left(\dfrac{AS_{min}}{AS_{mid}}\right)^{\frac{\tau-\tau_{max}/2}{\tau_{max}/2}}, & \tau > \dfrac{\tau_{max}}{2} \end{cases} \quad (44)$$

where $AS_{min} < AS_{mid} < AS_{max}$

When there is also a very small AS value for the region including an ideal global solution, the DE will start focusing all efforts on the use of the high- precision solution in the discovered region.

Integrating the mutation and crossover operations: In the standard DE, whether the crossover operation is carried out on $\left(u_{ij}^{\tau}\right)$ or not, the mutation operation is always performed on each variable $\left(u_{ij}^{\tau}\right)$ of target vector $\left(u_i^{\tau}\right)$ so as to generate the donor vector $\left(mu_{ij}^{\tau}\right)$. However, usually, there are only part of values in $\left(mu_{ij}^{\tau}\right)$ could be adopted in trial vector $\left(co_{ij}^{\tau}\right)$, which is as follow $co_{ij}^{\tau+1} = \begin{cases} mu_{ij}^{\tau+1}; & \left(rand(j) \le CR\right) or \left(j = J\right) \\ u_{ij}^{\tau}; & \text{Otherwise} \end{cases}$ (45)

3.3 Constraints repairing mechanism

In this paper, the inequality constraints are integrated into the fitness function using the penalty function approach. The objective function is to minimize expected system operating cost. Once the N-1 criteria is violated, the objective function is multiplied by a penalty factor equal to the square of the variable's violated value, and any infeasible solution obtained is rejected [40], which is expressed as:

$$\begin{aligned} ESC = {} & GC + WC + SC + BC + CC + \lambda_P * \sum_{t=1}^{T}\sum_{i=1}^{N_G}\left(P_{G_i,t} - P_{G_i}^{\lim}\right)^2 + \lambda_w * \sum_{t=1}^{T}\sum_{i=1}^{N_w}\left(P_{w,t} - P_w^{\lim}\right)^2 \\ & + \lambda_{PV} * \sum_{t=1}^{T}\sum_{i=1}^{N_w}\left(P_{s,t} - P_s^{\lim}\right)^2 + \lambda_Q * \sum_{t=1}^{T}\sum_{i=1}^{N_G}\left(Q_{G_i,t} - Q_{G_i}^{\lim}\right)^2 + \lambda_V * \sum_{t=1}^{T}\sum_{L=1}^{N_L}\left(V_{L,t} - V_L^{\lim}\right)^2 \\ & + \lambda_S * \sum_{t=1}^{T}\sum_{l=1}^{N_{trl}}\left(S_{l,t} - S_l^{\max}\right)^2 + \lambda_L * \sum_{t=1}^{T}\sum_{L=1}^{N_L}\left(L_{L,t} - L_L^{\lim}\right)^2 + \lambda_b * \sum_{t=1}^{T}\sum_{b=1}^{N_{batt}}\left(SOC_{b,t} - SOC_b^{\lim}\right)^2 \\ & + \lambda_{VD} * \sum_{t=2}^{T}\sum_{y=1}^{N_C}\left(V_{D_y,t} - V_{D_y}^{\lim}\right)^2 + \lambda_{TD} * \sum_{t=1}^{T}\sum_{y=1}^{N_C}\left(k_{D_y,t} - k_{D_y}^{\lim}\right)^2 + \lambda_{AD} * \sum_{t=1}^{T}\sum_{y=1}^{N_C}\left(\phi_{D_y,t} - \phi_{D_y}^{\lim}\right)^2 \end{aligned} \quad (46)$$

where the penalty factors for ramp-rate limits, wind power limits, solar power limits, reactive power limits, voltage limits, line-loading limits, line voltage stability limits, battery storage limits, dc voltage limits, converter transformer ratio limits, trigger angle or extinction angle limits are λ_P, λ_w, λ_{PV}, λ_Q, λ_V, λ_S, λ_L, λ_b, λ_{VD}, λ_{TD} and λ_{AD}.

The limit value of the dependent variable u is u^{lim} is provided as:

$$u^{\lim} = \begin{cases} u_{max} & u > u_{max} \\ u_{min} & u > u_{max} \end{cases} \quad (47)$$

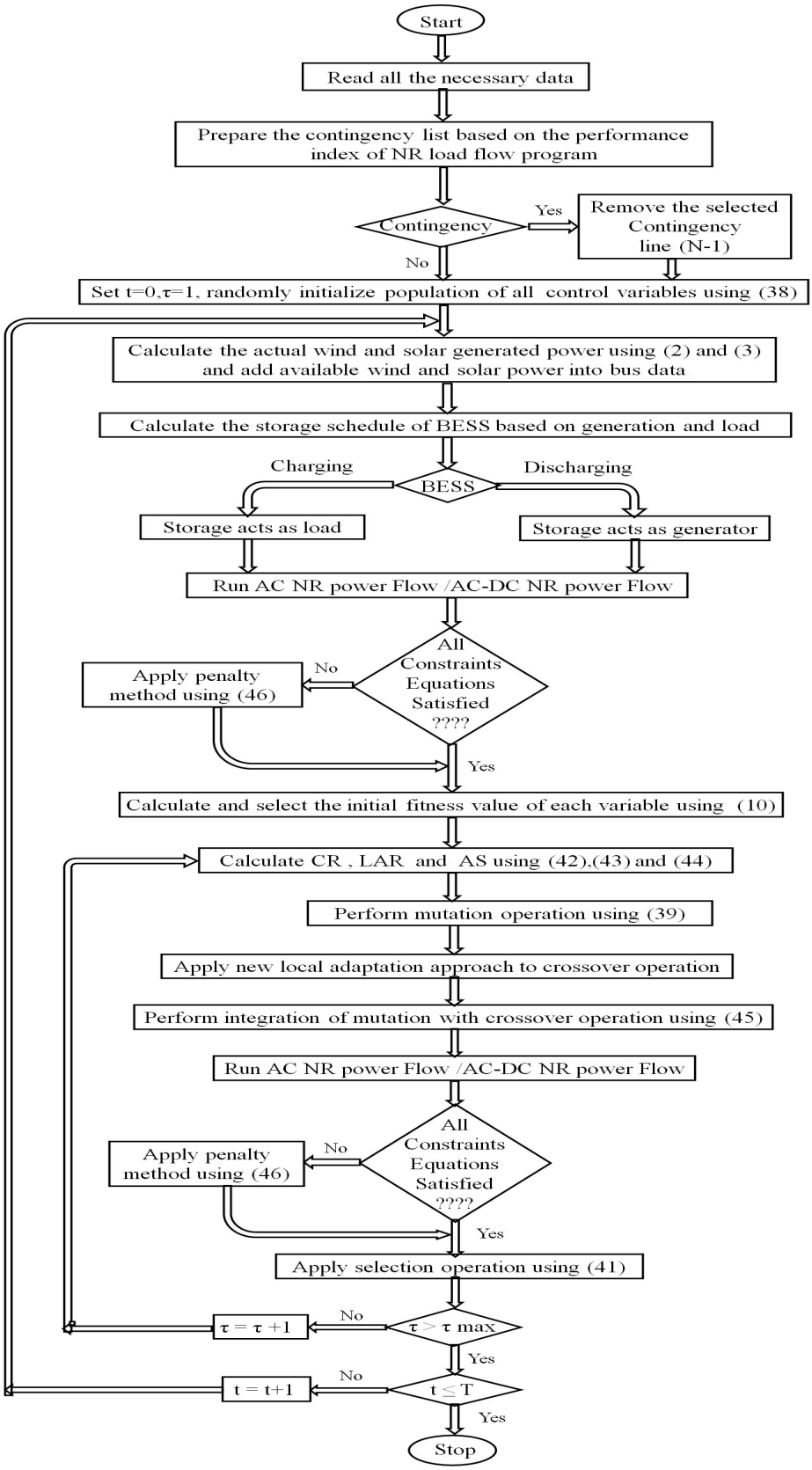

Figure 1. Flow chart of proposed NDE algorithm based ESCDOPF with RER and FR

4 Simulation results and discussions

In this paper, the proposed NDE algorithm has been implemented in the MATLAB-2016 version and evaluated on an IEEE-30 bus system, to validate its potential. In implementing the proposed NDE algorithm, the following NDE control parameters were set through experiment as follows: dimension of problem (M) = 11, population size (N_{pop}) =5, number of iterations (τ_{max}) =500, mutation factor (Fs) =0.5, CR_{max} =100/M, CR_{min} =30/M, LAR_{max} =0.99, LAR_{min} =0.1, AS_{max} =(u_{max}-u_{min})/10, ASmid =(u_{max}-u_{min})/(1E+4), ASmin =(u_{max}-u_{min})/(1E+15).

To compare the outcomes of the proposed NDE algorithm with other existing heuristic algorithms, we first addressed the DOPF problem that has been solved in prior works. This enables us to compare our findings with the existing literature to better illustrate the effectiveness of the proposed NDE approach. This research then solves the ESCDOPF problem without and with RER for different scenarios and different case studies with the NDE algorithm. The results are then compared to those from other case studies developed for each scenario in this study.

To assess the performance of the proposed NDE algorithm for the DOPF problem, we compared it to the conventional DE and other heuristic algorithms that used quadratic fuel cost with valve-point effect as an objective function over a 24-hour time horizon. The proposed NDE for the conventional DOPF problem yields a global fuel cost of 16,496 $/day. When compared to DE with different population sizes and previous literature findings, the proposed NDE has achieved the best solution with a smaller population size and less computational time, as shown in **Table 1**. As illustrated in **Figure 2**, the proposed NDE algorithm outperforms the standard DE with different population sizes and other literature findings in terms of obtaining the best value of fuel cost of 16,496 $/day over 500 iterations.

TABLE 1. Comparison of conventional DOPF generation cost with all the constraints

Method	Fuel Cost ($/day)	time (sec)
SA [3]	16,703.81	1408.46
PSO [3]	16,619.92	811.69
DE (Npop=30)	16,522.99	392.02
DE (Npop=40)	16,509.34	533.35
DE (Npop=50)	16,505.82	666.95
NDE (proposed)	**16,496.00**	**128.06**

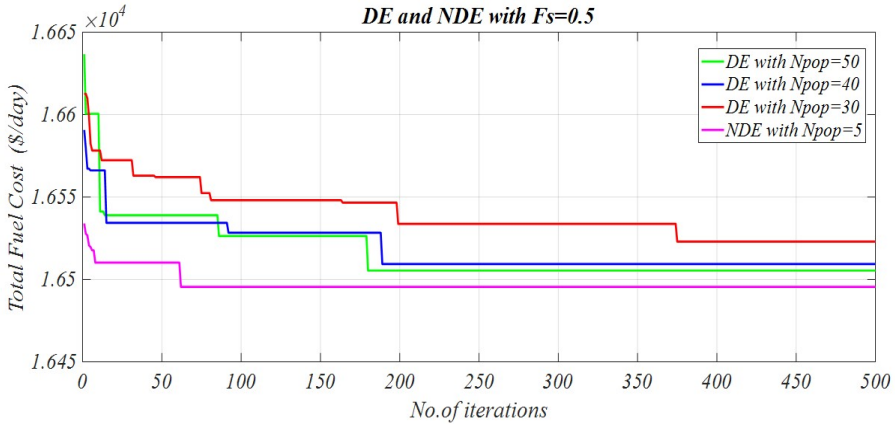

Figure 2. DOPF fuel cost convergence characteristics

4.1 ESCDOPF problem

To study the performance of the proposed NDE based ESCDOPF model, two scenarios are considered as below:

a) Scenario-A: ESCDOPF with FR during normal (N) and post-contingency (PC) states
b) Scenario-B: ESCDOPF with RER and FR during normal (N) and post-contingency (PC) states

To investigate the performance without/with RER and FR on the operation of the proposed NDE based ESCDOPF model in all scenarios, different cases are considered for each scenario, as given below.

1. Case # 1: Base case (all FRs are ignored)
2. Case # 2: With MT HVDC only
3. Case # 3: With BESS only
4. Case # 4: With both BESS and MT HVDC

***a) SCENARIO-A:* ESCDOPF with FR during normal (N) and post-contingency (PC) states**

In this paper, the complete IEEE 30 bus system data along with generator fuel cost, consumer benefit cost, forecasted load demand, ramp rate limits and all other data are extracted from [3, 42]. Additionally, on bus 14, a 100 MWh BESS with a battery SOC that can range from 40% to 100% of the rated battery capacity is installed. Both the charging and discharging efficiencies of η_{ch_b} and η_{dch_b} are set to 90%. The battery power limits are set to $0 \leq P_b \leq 15$ MW. The h_b is assumed to be 1.0 Rs/MWh. In extension with the existing proposed ESCDOPF model, this scenario considers a multi-terminal (MT)-HVDC lines. The DC data for the MT-HVDC link that has mesh connected between HVDC -1 (2 and 7), HVDC-2 (5 and 7), and HVDC-3 (2 and 5), can be found in [28].

From the actual forecasted load demand [3], the peak load hours have been chosen at 18:00-20:00 hours, respectively. The storage schedules are determined based on the generation limits of all the generators and load demand. By proper selection of charging and discharging hours, the BESS would act either as a variable load or a generator, depending on whether to absorb surplus active power or to provide deficit active power. When the BESS is used, the total charging power is greater than the total discharging power. Due to this, there is a reduced peak load of power. Because of reduced peak load power, the size of system equipment, and the reserve capacity of the system are reduced.

Furthermore, a single transmission line outage was used to include a contingency in this simulation. Using bus 1 as a reference, 36 "N-1" contingencies are defined in which islanding circuits are excluded. The line-loading and voltage limits are set to 120% and 5%, respectively, of the standard case values, respectively. In this work, the performance index is measured by the NR load flow (NRLF) approach, which was used to rank the contingencies [18]. Only five contingencies are considered, each representing the outage of lines along with their performance indexes: 6-8 (497.3), 6-28 (230.20), 28-27 (131.21), 10-21 (82.58), and 11-12 (62.73). Here, in x(y), x as the line outage and y as the severity index. Following a security review, it was discovered that the outage of the line connecting buses 6-8 creates a most severe contingency situation in the network.

The proposed NDE algorithm is used to tackle the ESCDOPF problem of performing preventive control actions, such as generator rescheduling, to return the system to its original state while satisfying model constraints. Moreover, SOC of BESS along with the operational time frame is included in the ESCDOPF during normal and post-contingency states of cases 3 and 4 as shown in **Figure 3**. Indeed, by storing energy during the off-peak phase and switching to the discharge mode during peak hours, the BESS units have reduced the need for conventional generation units during peak hours. This has also resulted in a decrease in operational costs.

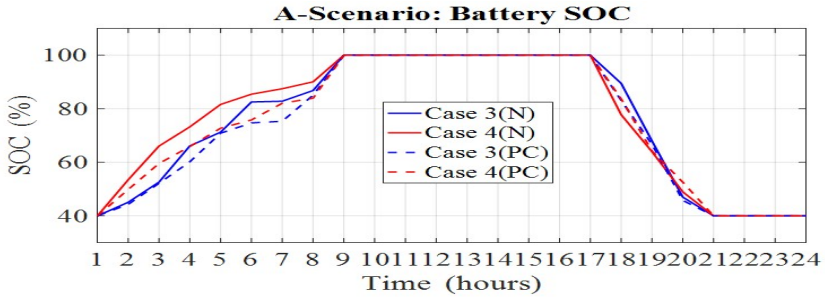

Figure 3. Scenario-A: SOC under normal (N) and post-contingency (PC) states.

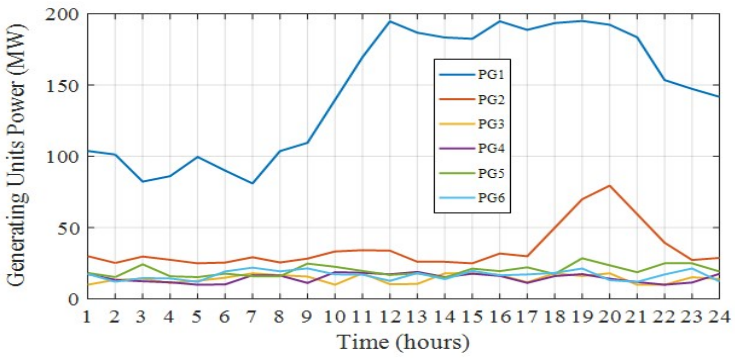

Figure 4. Scenario-A: Optimal power scheduling of the generating units for 24 hours

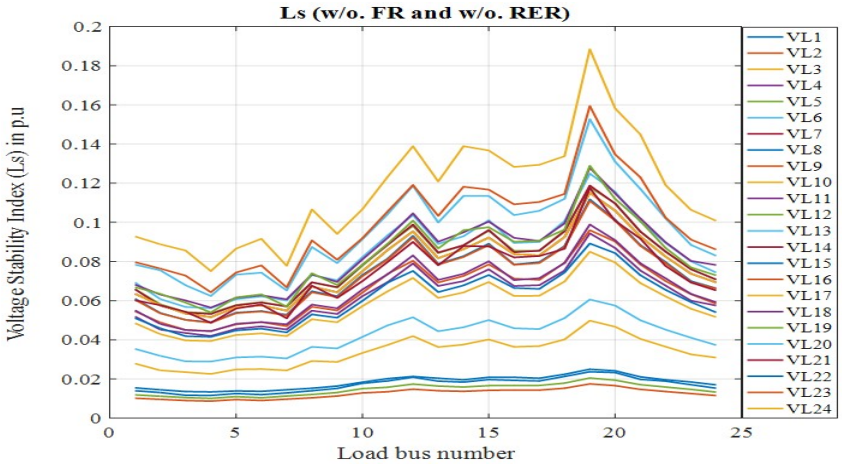

Figure 5. Scenario-A: Voltage stability indices for base case

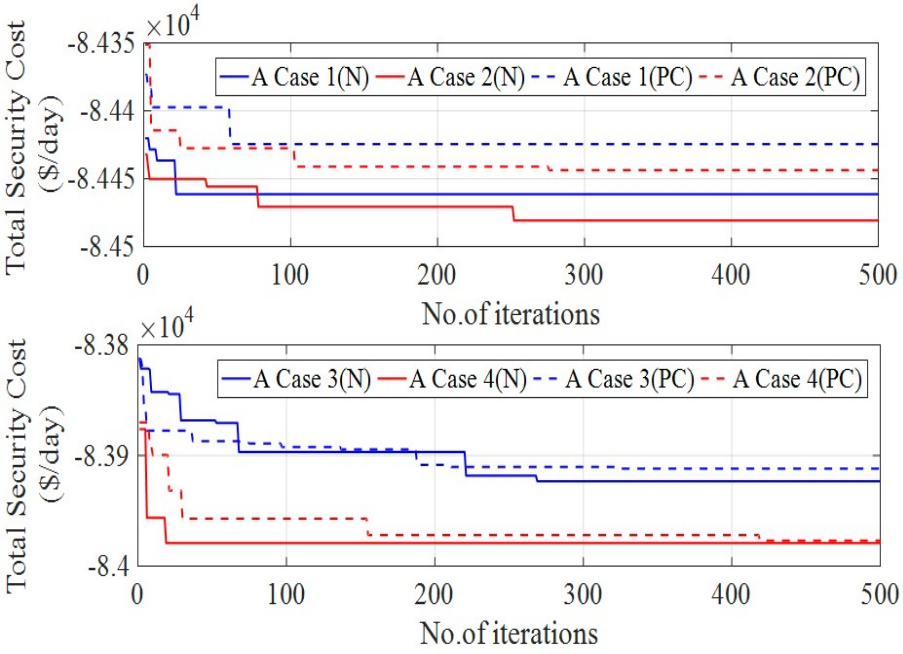

Figure 6. Scenario-A: Cost-convergence characteristics of all cases under normal (N) and post-contingency (PC) states.

Table 2. Scenario-A: Final results of MTHVDC

MT-HVDC Final values	V_{DR} (p.u)	k_{DR}	α_R (deg)	V_{DI} (p.u)	k_{DI}	γ_I (deg)	P_{DR} (MW)	Q_{DR} (MVAR)	P_{DI} (MW)	Q_{DI} (MVAR)	I_D (pu)
HVDC-1	1.2858	0.947	8	---	---	---	56.10	16.10	---	---	0.436
HVDC-2	1.286	0.959	12.7	---	---	---	61.70	15.9	---	---	0.48
HVDC-3	---	---	---	1.279	1.01	22	---	---	117.20	54.2	0.916

Table 3. Scenario-A: Comparison results of all cases under normal (N) and post-contingency states (PC)

Scenario-A	Case 1		Case 2		Case 3		Case 4	
	N	PC	N	PC	N	PC	N	PC
Total fuel Cost ($/day)	16496.00	16535.62	16479.23	16516.34	16428.45	16406.49	16409.11	16373.60
Total Benefit Cost ($/day)	100960.0	100960.0	100960.0	100960.0	100960.0	100960.0	100960.0	100960.0
Total Storage Cost ($/day)	---	---	---	---	608.27	641.67	571.86	609.64
Total Security Cost ($/day)	-84464.00	-84424.38	-84480.77	-84443.66	-83923.28	-83911.84	-83979.03	-83977.36
Total Power Loss (MW/day)	186.89	194.18	180.47	187.68	181.55	188.21	171.40	179.78
Time (sec)	168.88	168. 77	282.71	282.30	134.44	134.43	194.76	195.21

The DC control parameters solution values and the corresponding powers at the converters are given in **Table 2**. The final results for total security cost, power losses and their computational times in all cases under normal and post-contingency states are given in **Table 3.** Optimal power scheduling of generating units for base case (i.e., case 1) is shown in **Figure 4**. Also, the voltage stability index for the load bus voltages is shown in **Figure 5**. The comparison convergence characteristics of total security costs for Scenario-A of all cases during normal-and-post contingency states are shown in **Figure 6**.

Analyzing the results in **Table 3**, it is observed that the proposed algorithm reduces the total generator fuel cost and power losses with the incorporation of FR. Nonetheless, by observing the total security costs (TSC) in **Table 3**, a reduction is observed. However, TSC is not as reduced in cases 3 and 4 as compared to cases 1 and 2. This is expected due to the inclusion of battery storage costs.

b) Scenario-B: ESCDOPF with RER and FR

This scenario investigates the effects of RER and FR on the ESCDOPF of the proposed NDE algorithm. The modified IEEE 30 bus system is employed to accommodate wind and solar farms with a total capacity of 40 MW and 20 MW, respectively, located on buses 22 and 24, which are depicted arbitrarily in **Figure 7**.

The wind speed and solar irradiance information with hourly resolution are accessible on the National Renewable Energy Laboratory (NREL) webpage [43]. Using the least square method (LSM) and the graphical method, the scale factor (s_c) and shape factor (s_k) of the Weibull distribution are estimated at 6.1589 and 4.0381, respectively. The parameters of the Beta distribution are estimated at 2.9721 and 8.9928 as scale factor (a_s) and shape factor (b_s).

Therefore, the actual forecasted wind ($P_{w,act}$) and solar power ($P_{s,act}$) is plotted in **Figure 8**. It is assumed that wind and solar power forecasts are affected by an adequate error in order to achieve wind and solar power generation. As a random variable, the maximum wind and solar power fluctuations are taken to be 20% of the predicted. Then wind and solar power are considered schedulable. The parameters of the wind velocities $(v_{\text{in}}, v_{\text{out}}, \text{ and } v_{\text{wr}})$ are 3 m/s, 20 m/s and 10.28 m/s, respectively. The PV module specifications for solar energy conversion can be found in [12]. The cost-coefficients of wind generators are K_w = 8 Rs/MWh, K_{pw} = 1.5 Rs/MWh, and K_{rw} = 10 Rs/MWh respectively. The cost-coefficients of solar generators are K_s =9 Rs/MWh, K_{ps} = 1.5 Rs/MWh, and K_{rs} = 11 Rs/MWh respectively.

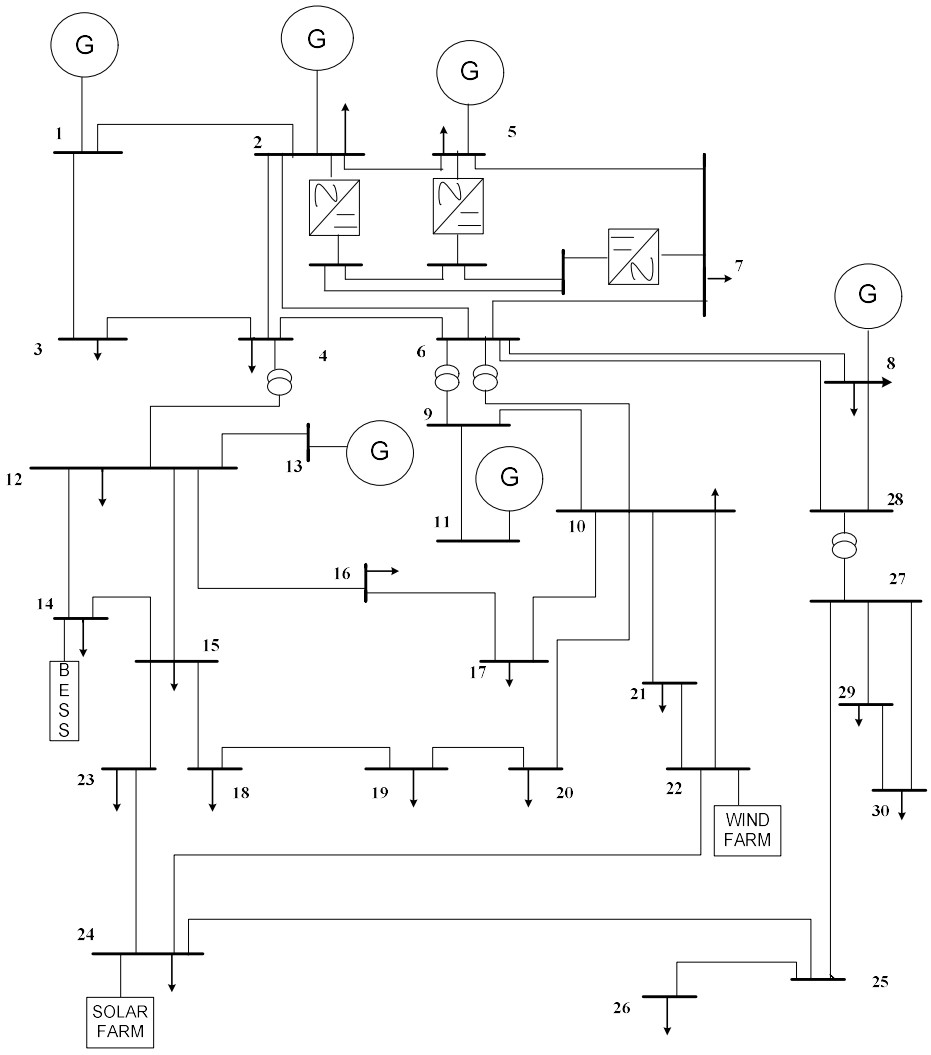

Figure 7. Modified IEEE-30 bus system with RER and FR

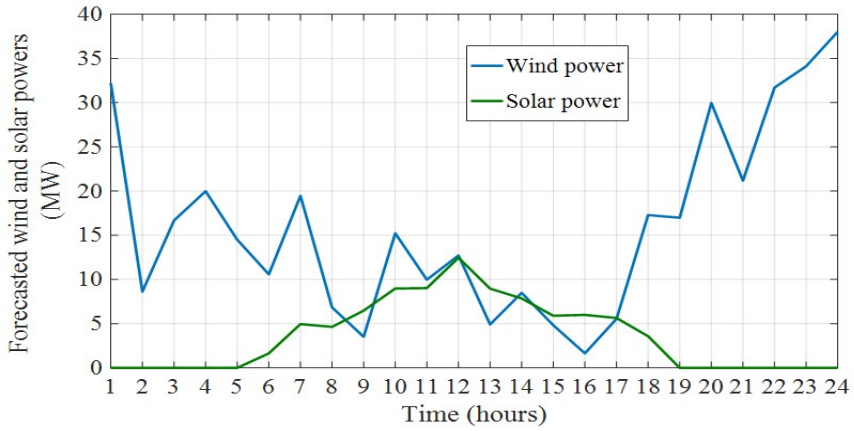

Figure 8. Actual forecasted wind and solar power generations

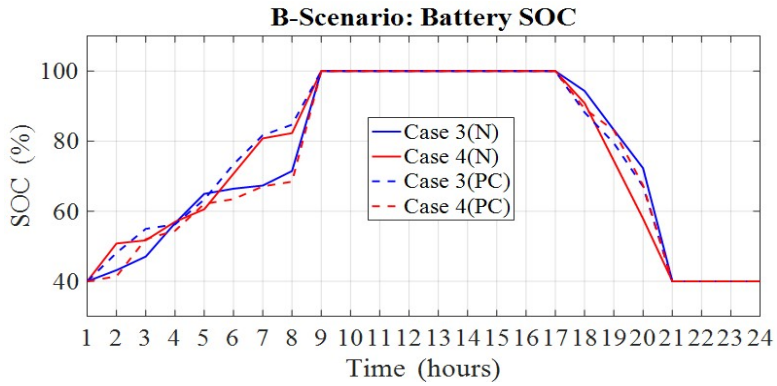

Figure 9. Scenario-B: SOC under normal (N) and post-contingency (PC) states.

As noted previously and illustrated in **Figure 9**, the BESS operation has a large impact on the total security cost and its SOC conditions during normal and post-contingency states, respectively. The DC control parameters solution values and powers at the converters are given in **Table 4**. The results obtained from the MT-HVDC link show that the proposed NDE approach enables the study of the effects of DC on the AC power flows during pre- and post-contingency states. This observation is delineated in **Table 5** with their power losses and computational times**. Figure 10** shows the output of conventional generating units including RERs, for each hour for the base case. Also, the voltage stability index for the load buses is shown in **Figure 11**. The comparison convergence characteristics of total security costs for Scenario-B of all cases during normal-and-post contingency states are shown in **Figure 12**.

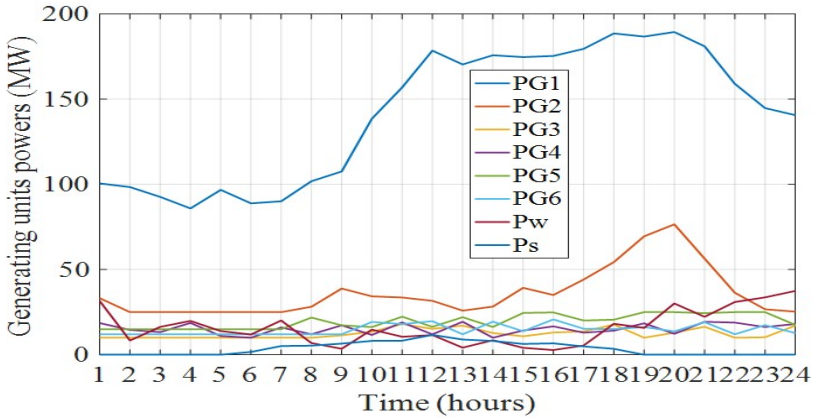

Figure 10. Scenario-B: Optimal power scheduling of the generating units for 24 hours

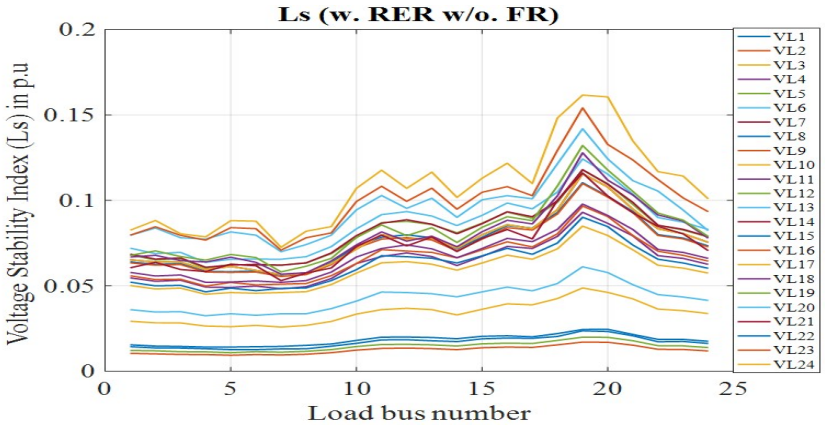

Figure 11. Scenario-B: Voltage stability indices for DOPF model

Table 4. Scenario-B: Final results of MTHVDC (base case)

MT-HVDC Final values	V_{DR} (p.u)	k_{DR}	α_R (deg)	V_{DI} (p.u)	k_{DI}	γ_I (deg)	P_{DR} (MW)	Q_{DR} (MVAR)	P_{DI} (MW)	Q_{DI} (MVAR)	I_D (pu)
HVDC-1	1.27	0.961	8	---	---	---	55.4	15.90	---	---	0.436
HVDC-2	1.272	0.915	12.7	---	---	---	61.10	12.10	---	---	0.48
HVDC-3	---	---	---	1.267	0.996	22	---	---	116.10	53.8	0.916

Table 5. Scenario-B: Comparison results of all cases under normal (N) and post-contingency states (PC)

Scenario-B	Case 1		Case 2		Case 3		Case 4	
	N	PC	N	PC	N	PC	N	PC
Wind direct cost ($/day)	3023.00	3033.20	3052.60	3028.20	3045.20	3054.00	3044.80	2981.30
Wind penalty cost ($/day)	16.78	15.04	13.13	23.53	17.26	19.75	17.49	23.86
Wind reserve cost ($/day)	40.82	41.96	53.57	38.87	71.74	43.15	50.31	35.84
Solar direct cost ($/day)	758.91	764.73	715.25	711.91	740.98	701.88	710.51	733.43
Solar penalty cost ($/day)	19.94	6.76	13.10	13.37	16.90	15.73	10.68	12.34
Solar reserve cost ($/day)	43.35	37.07	35.44	32.15	21.33	37.93	31.43	39.80
Total fuel cost ($/day)	15984.00	16050.00	15930.00	16009.00	15864.00	15857.00	15834.00	15815.00
Total battery cost ($/day)	---	---	---	---	633.16	600.8	623.02	651.37
Total benefit cost ($/day)	100960	100960	100960	100960	100960	100960	100960	100960
Total security cost ($/day)	-81073.20	-81011.24	-81146.91	-81102.97	-80549.43	-80629.80	-80637.76	-80667.06
Total losses (MW/day)	173.95	177.60	168.50	172.98	169.29	165.15	164.07	169.76
Time (sec)	88.568	89.178	262.211	283.298	86.921	87.199	260.388	254.947

Analysing the results of Scenario-B, it is observed that in all cases, the total operation costs are reduced due to the incorporation of FR. Nonetheless, by observing the total security costs (TSC) in **Table 5**, a reduction is observed.

However, TSC is not as reduced in cases 3 and 4 as compared to cases 1 and 2. This is expected due to the inclusion of battery storage costs.

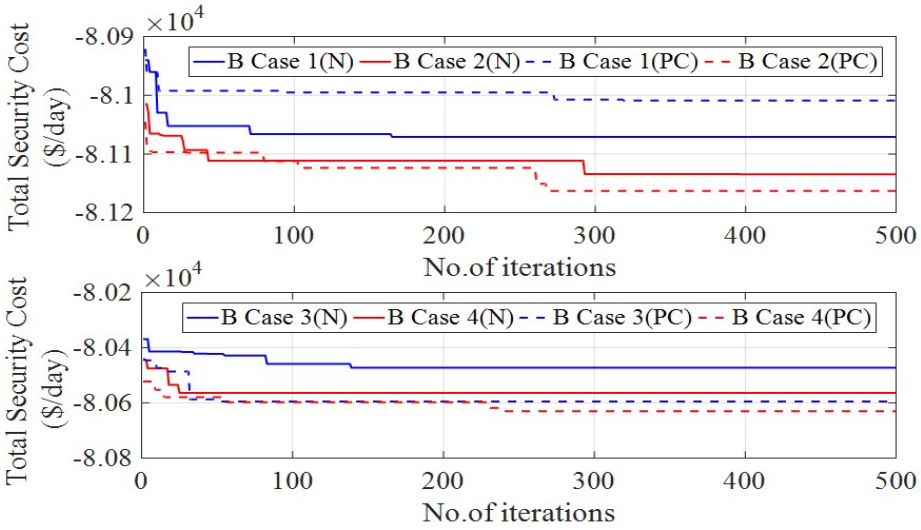

Figure 12. Scenario-B: Cost convergence characteristics of all cases in normal (N) and post- contingency (PC) states.

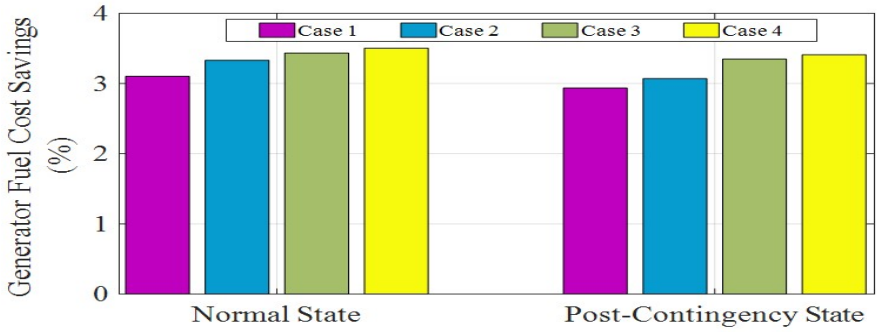

Figure 13. Comparison of generator fuel cost savings

When the results of Scenarios A and B are analysed, it is clear that the total expected operation costs are reduced in all situations due to the inclusion of RER and FR. Also, when Scenario-A is compared to Scenario-B, it is evident that with the integration of RER and FR, the generator fuel cost is reduced in all cases. The percentage fuel cost savings are observed as 3.1037 (2.9368) %, 3.3328 (3.0717) %, 3.4358 (3.3492) %, 3.5048 (3.4115) when compared to all cases in normal and post- contingency conditions, as shown in **Figure 13**. Here, in x(y), x as the percentage fuel cost savings in normal state and y as the post-contingency cost savings. On the contrary, generator fuel costs are decreasing significantly, indicating a promising development in non-conventional resources.

5. Conclusions

This paper develops a new ESCDOPF model that includes renewable energy resources (RER) and flexible resources (FR) to show how these resources affect expected system operating cost. The uncertainties of the RERs have been modelled using Weibull and Beta PDFs. This study also confirms the idea that BESS is more useful not only for temporary energy shifts but also for reliability purposes. To enhance grid flexibility, MT LCC-HVDC systems are used as a fast-controlling device. A Novel DE (NDE) algorithm for an IEEE-30 bus system has been devised to address the ESCDOPF problem in the presence of RER and FR. Furthermore, the proposed NDE algorithm for the standard DOPF problem is compared to the standard DE and other existing algorithms to overcome the limitations of the standard DE approach, and a good result was reported with less convergence time and population size. The proposed NDE algorithm for the ESCDOPF problem was evaluated in two scenarios in both normal and post-contingency states. According to

the technical findings, the presence of RER and FR provides significant benefits, such as reduction in peak load, power losses and generation costs. In all test scenarios, the proposed NDE algorithm offers cost savings and promising solutions to achieve secure, reliable, cost-effective operations and good convergence performance.

Acknowledgements

This work is supported by the Ministry of electronics & information technology (MeitY), Government of India (GOI) through Visvesvaraya Ph.D. scheme under Grant MEITY-PHD-2352.
The authors are also thankful to the SERB, Government of India for providing infrastructure facilities under TARE research project (TAR/2018/000390).

References

[1] K. Morison, L. Wang and P. Kundur, “Power System Security Assessment”, IEEE Power & Energy Magazine, pp. 30-39, Sept./Oct.2004.
[2] O. Alsac and B. Stott, “Optimal load flow with steady state security, IEEE Trans. Power App. Syst., vol. PAS-93, no. 3, pp. 745–751, Mar. 1974.
[3] T. Niknam, MR Narimani, M Jabbari, "Dynamic optimal power flow using hybrid particle swarm optimization and simulated annealing,” Int. Trans. on Elec. Energy Systems 23 (7), 975-1001, 2013.
[4] Saber Armaghani, Nima Amjady, Oveis Abedinia, “Security constrained multi-period optimal power flow by a new enhanced artificial bee colony”, Applied Soft Computing, vol. 37, Pages 382-395, 2015.
[5] F. Capitanescu, J.L. Martinez Ramos, P. Panciatici, D. Kirschen, A. Marano Marcolini, L. Platbrood, L. Wehenkel, State-of-the-art, challenges, and future trends in security constrained optimal power flow, Electric Power Systems Research, Volume 81, Issue 8, Pages 1731-1741, 2011.
[6] Y. Xu, Z. Y. Dong, R. Zhang, K. P. Wong and M. Lai, "Solving Preventive-Corrective SCOPF by a Hybrid Computational Strategy," in IEEE Trans. on Power Systems, vol. 29, no. 3, pp. 1345-1355, May 2014.
[7] Galvani, S., Talavat, V., & Rezaeian Marjani, S. “Preventive/Corrective Security Constrained Optimal Power Flow Using a Multi objective Genetic Algorithm”. Elect. Power Comp. and Sys., 1–16, 2018.
[8] J. Condren, T. W. Gedra, and P. Damrongkulkamjorn, “Optimal power flow with expected security costs,” IEEE Trans. Power Syst., vol. 21, no. 2, pp. 541–547, May 2006.
[9] J. Condren and T. W. Gedra, “Expected-security-cost optimal power flow with small-signal stability constraints,” IEEE Trans. Power Syst., vol. 21, no. 4, pp. 1736–1743, Nov. 2006.
[10] Qazi, A., Hussain, F., Rahim, N. A., Hardaker, G., Alghazzawi, D., Shaban, K., & Haruna, K. “Towards Sustainable Energy: A Systematic Review of Renewable Energy Sources, Technologies, and Public Opinions”, IEEE Access, 7, 6383 63851, 2019. doi:10.1109/access.2019.2906402.
[11] Surender Reddy, S., Bijwe, P. R., & Abhyankar, A. R. “Real-Time Economic Dispatch Considering Renewable Power Generation Variability and Uncertainty Over Scheduling Period”. IEEE Systems Journal, 9(4), 1440–1451, 2015. doi:10.1109/jsyst.2014.2325967.
[12] Jadoun, V. K., Pandey, V. C., Gupta, N., Niazi, K. R., & Swarnkar, A. “Integration of renewable energy sources in dynamic economic load dispatch problem using an improved fireworks algorithm”. IET Rene. Power Gen., 2018,12(9), 1004–1011.
[13] P. P. Biswas, P. N. Suganthan, and G.A.J. Amaratunga, ‘‘Optimal power flow solutions incorporating stochastic wind and solar power”, Energy Convers. Manage., vol. 148, pp. 1194–1207, Sep. 2017.
[14] Chamanbaz M, Dabbeney F, Lagoaz C, “AC optimal power flow in the presence of renewable sources and uncertain loads”, IEEE Trans Power Syst, 1–22,2017.
[15] Kathiravan R, Kumudini Devi RP, “Optimal power flow model incorporating wind, solar, and bundled solar-thermal power in the restructured indian power system”. Int J Green Energy, 2017, 14(11):934–950.
[16] Khan B, Singh P, “Optimal power flow techniques under characterization of conventional and renewable energy sources: a comprehensive analysis”. J Eng Hindawi, 1–16, 2017.
[17] Syed, M.S., Chintalapudi, S.V., & Sirigiri, S. “Optimal Power Flow Solution in the Presence of Renewable Energy Sources”. *Iranian Journal of Science and Technology, Transactions of Electrical Engineering, 45, 61-79,2020.*
[18] Teeparthi K, Vinod Kumar DM, “Multi-objective hybrid PSO– APO algorithm-based security constrained optimal power flow with wind and thermal generators”. Eng Sci Technol Int J 20(2):411–426, 2017.
[19] O.M. Babatunde, J.L. Munda, Y. Hamam, Power system flexibility: A review, Energy Reports, Volume 6, Supplement 2, Pages 101-106, 2352-4847, 2020, https:// doi.org /10.1016/j.egyr.2019.11.048.
[20] M. Chandy, S. Low, U. Topcu, and H. Xu, “A simple optimal power flow model with energy storage,” Proc. of Conf. on Decision and control, pp. 1051-1057, 2010.
[21] Zhongwei Wang, Jin Zhong, Dong Chen, Yuefeng Lu and Kun Men, "A multi-period optimal power flow model including battery storage," 2013 IEEE *Power & Energy Society General Meeting*, pp.1-5,2013. doi: 10.1109/PESMG.2013.6672498.
[22] J. K. Felder and I. A. Hiskens, "Optimal power flow with storage," *2014 Power Systems Computation Conference*, 2014, pp. 1-7, doi: 10.1109/PSCC.2014.7038334.
[23] Chen, T., Jin, Y., Lv, H. et al. Applications of Lithium-Ion Batteries in Grid-Scale Energy Storage Systems. Trans. Tianjin Univ. 26, 208–217,2020. doi: 10.1007/s12209-020-00236.
[24] J. Cao, W. Du, and H. Wang, “An Improved Corrective Security -Constrained OPF With Distributed Energy Storage,” *IEEE Trans. on Power Sys.*, vol. 31, no. 2, pp. 1537–1545, March 2016.
[25] Gill, S., Kockar, I., & Ault, G. W. “Dynamic Optimal Power Flow for Active Distribution Networks”. IEEE Transactions on Power Systems, 2014, 29(1), 121–131. doi:10.1109/tpwrs.2013.2279263.
[26] M. I. Alizadeh, M. Usman and F. Capitanescu, "Toward Stochastic Multi-period AC Security Constrained Optimal Power Flow to Procure Flexibility for Managing Congestion and Voltages," 2021 International Conference on Smart Energy Systems and Technologies (SEST), 2021, pp. 1-6.
[27] T. Smed, G. Andersson, G. B. Sheble and L. L. Grigsby, "A new approach to AC/DC power flow," in IEEE Transactions on Power Systems, vol. 6, no. 3, pp.1238-1244, Aug. 1991.
[28] G. Durga Prasad, P. Seshagiri Rao,"A heuristic method for the real-time load flow solution of integrated multiterminal AC-DC power systems”, Electric Power Systems Research, Volume 28, Issue 2, Pages 139-147, 1993.
[29] Wang XF, Fang WL, Du ZC. Modern power system analysis. Beijing: Science Press; 2003. p. 180–201.

[30] A. Rabiee, A. Soroudi and A. Keane, "Information Gap Decision Theory Based OPF With HVDC Connected Wind Farms," in IEEE Trans. on Power Systems, vol. 30, no. 6, pp. 3396-3406, Nov. 2015.
[31] Best Paths. Beyond state-of-the-art technologies for power AC corridors and multi-terminal HVDC systems, European Union Horizon 2020 research and innovation programme, project ID: 612748. http://www.bestpaths-project.eu/.
[32] Jia Cao, Zheng Yan, Jianhua Li, Lu Cao, "Impact of HVDC line on the convergence property of AC/DC power flow calculation", International Journal of Electrical Power & Energy Systems, Volume 83, 2016, Pages 140-148, ISSN 0142-0615.
[33] Huebner. N, Schween N, Suriyah. M, H. Vincent, L. Thomas, "Multi-area Coordination of Security-Constrained Dynamic Optimal Power Flow in AC-DC Grids with Energy Storage, Advances in Energy System Optimization, 27- 40, Springer International Publishing, 2020.
[34] Storn R., Price K., "Differential evolution – a simple and efficient heuristic for global optimization over continuous spaces', J Global Optim., 1997, 11, pp. 341– 359.
[35] A.A. Abou El Ela, M.A. Abido, S.R. Spea, Optimal power flow using differential evolution algorithm, Electric Power Systems Research, Volume 80, Issue 7,2010, Pages 878-885, ISSN 0378-7796.
[36] S.Das and P. N. Suganthan, "Differential Evolution: A Survey of the State-of-the-Art," in IEEE Transactions on Evolutionary Computation, vol. 15, no. 1, pp. 4-31, Feb. 2011.
[37] Cai Z, Gong W, Ling CX, Zhang H, "A clustering-based differential evolution for global optimization". Appl Soft Comput 11(1):1363–1379, 2011.
[38] Wang Y, Cai Z, Zhang Q, Enhancing the search ability of differential evolution through orthogonal crossover. Inf Sci 185(1):153-177, 2012.
[39] Yinzhi Zhou, Xinyu Li, Liang Gao, A differential evolution algorithm with intersect mutation operator, Applied Soft Computing, Volume 13, Issue 1, Pages 390-401, 2013, ISSN 1568-4946.
[40] Vaisakh, K., & Srinivas, L. R. Evolving ant direction differential evolution for OPF with non-smooth cost functions. Engineering Applications of Artificial Intelligence, 2011, 24(3), 426–436. doi: 10.1016/j.engappai.2010.10.019.
[41] Shouheng Tuo, Junying Zhang, Xiguo Yuan, Longquan Yong, "A new differential evolution algorithm for solving multimodal optimization problems with high dimensionality". Soft Comp. 22(13):4361-4388, 2018.
[42] Arsalan, Q." Expected Security Cost Optimal Power Flow Using Parallel and Distributed computation", Ph.D. dissertation, Oklahoma, USA, 2007.
[43] National Renewable Energy Laboratory (NREL). Available at www.nrel.gov.